DOI: 10.58895/ksp/1000128686-10 erschienen in:
OCM 2021 - 5th International Conference on Optical Characterization of Materials, March 17th – 18th, 2021, Karlsruhe, Germany : Conference Proceedings
DOI: 10.58895/ksp/1000128686 | https://www.ksp.kit.edu/site/books/m/10.58895/ksp/1000128686/

Measurement of the coefficient of linear thermal expansion based on subjective laser speckle patterns

Alexander Spaett[1] and Bernhard G. Zagar[1]

Johannes Kepler University Linz, Institute for Measurement Technology, Altenberger Straße 69, A-4040 Linz

Abstract We present an improved processing of laser speckle intensity signals aimed at attaining spatial displacement resolutions well in the sub-pixel domain, which is necessary for measuring the minute displacements caused by thermal expansion of metallic specimens. The signal processing revolves around the cross power spectral density and the coherence function of two discrete signals, which allows for a continuously varying displacement result as opposed to a discretized, if determined in the spatial domain via the application of the cross-correlation function. The presented technique is then applied to estimate the coefficient of linear thermal expansion (CLTE) of a brass sample.

Keywords Coefficient of linear thermal expansion, subjective laser speckles, strain measurement, displacement estimator, unbiased minimum variance estimator

1 Introduction

Laser speckle patterns are caused by the interference of coherent light reflected off an optically rough surface. When it comes to speckle imaging, one differentiates between subjective and objective laser speckle patterns. In the former an optical setup is used and the speckle pattern in the image plane is evaluated. The latter describes the speckle pattern in the object plane that is captured directly by a camera [1]. Successively captured one-dimensional speckle pattern can be seen in Fig. 4.1.

Although laser speckles are often an unwanted source of noise they can also be utilized in different applications, since they represent something similar to a fingerprint of the illuminated surface. For instance, the measurement of the shift of the imaged laser speckle pattern may be used to determine the surface strain of a sample. Knowledge about the surface strain, in turn, allows to deduce the coefficient of linear thermal expansion (CLTE).

The presented contactless method provides the possibility to measure mechanical properties of samples for which common approaches, like strain gauges, are not applicable. As an example one could name the measurement of strain of materials which are small in at least one dimension, e.g. natural fibres.

2 Speckle shift in the image and its relation to the CLTE

In order to give a better understanding of the digital signal processing applied, a theoretical model linking the speckle shift in the image with the CLTE of the sample will be reviewed. However, the following considerations will be limited to telecentric imaging systems. A broader treatment can be found in [2].

When a telecentric imaging system is used to observe the speckles, the speckle shift captured by a camera is given by the following equation first derived by Yamaguchi in 1981 [3]

$$A_y = \overbrace{\frac{a_x}{M}\frac{\Delta L}{L_S} l_{Sx} l_{Sy}}^{A_I} - \overbrace{\frac{a_y}{M}\left[1 + \frac{\Delta L}{L_S}(1 - l_{Sy}^2)\right]}^{A_{II}} + \overbrace{\frac{a_z}{M}\frac{\Delta L}{L_S} l_{Sx} l_{Sz}}^{A_{III}} + \underbrace{\frac{\Delta L}{M} \cdot \left(\varepsilon_{xy} l_{Sx} + \varepsilon_{yy} l_{Sy} - g(\Omega)\right)}_{A_{IV}} + E. \tag{2.1}$$

A_y describes the resulting shift of the laser speckle pattern in the image plane in y_I-direction and ε is the desired strain tensor of the sample. As can be seen, both the components ε_{xy} and ε_{yy} of the strain tensor can - in theory - be observed directly. Instead, in order to avoid multiple sources contributing to A_y, the shift a_y of the diffracting surface will be estimated. The strain in y-direction ε_{yy} can then be deduced

from this quantity. The general setup leading to Eqn. 2.1 is depicted in Fig. 2.1.

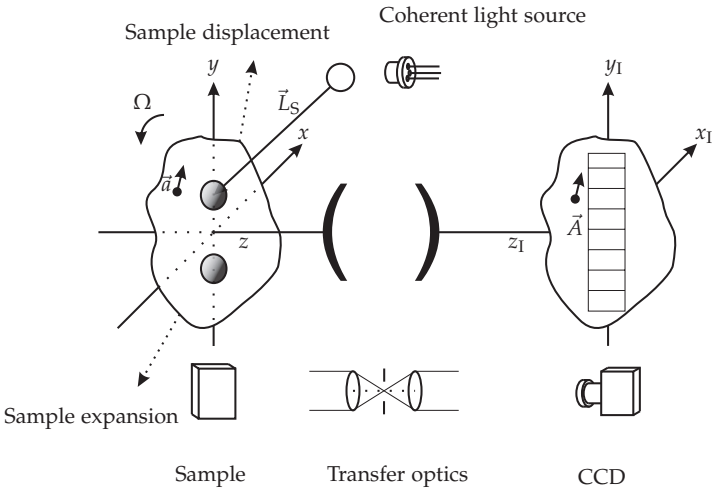

Figure 2.1: General geometrical setup for modelling the pattern shift in the image plane.

The sample lying in the x-y-plane on the left is illuminated by a coherent light source. The distance L_S then describes the distance between the ideal point source and the illuminated spot on the surface and therefore the radius of the curvature of the laser beam. The vector pointing from the source to the spot on the surface can be described by $\vec{L}_S = L_S \cdot \vec{l}_S$ with $\vec{l}_S = \begin{bmatrix} l_{Sx} & l_{Sy} & l_{Sz} \end{bmatrix}^T$ denoting the unit vector, representing the direction of the laser beam. The demagnification factor M, given by the optics used, as well as the distance between the focal plane of the telecentric optics and the sample ΔL influence the speckle shift in the image plane.

Tilting the sample also translates to a shift in the image. This is stated by the function g of the rotation vector Ω. The additional error term E summarizes non ideal or not sufficiently well known dimensional parameters, like temperature dependant expansion of the sensor and overall build-up, causing speckle pattern shifts not distinguishable from a true strain contribution [4].

When the strain estimation is solely based on a_y, it becomes evident that any term in Eqn. 2.1 but A_{II} is negatively influencing the accuracy of the estimate and hence should be minimized. By placing the sample near or ideally in the focus, both ΔL and $\frac{\Delta L}{L_s}$ become small, resulting in the contributions of A_I, A_{III} as well as A_{IV} to be negligible. The impact of A_I and partially A_{IV} can be reduced further by choosing the position of the coherent light source, which in our case is a laser diode (LD) with collimating optics, carefully. When the LD is placed at the same height, meaning having the same y-component, as the spot on the surface, then for the parameter l_{Sy} it follows $l_{Sy} = 0$.

Having taken all measures mentioned above, Eqn. 2.1 reduces to

$$A_y = -\frac{a_y}{M} + E. \tag{2.2}$$

For the calculation of the strain and the CLTE two vertically aligned laser spots are utilized. When $A_{y,Upper}$ is the shift that the upper spot experiences and $A_{y,Lower}$ the one of the lower spot, then the engineering strain can be described as

$$\varepsilon = \frac{-M \cdot (A_{y,Upper} - A_{y,Lower})}{d_{ul}}, \tag{2.3}$$

where d_{ul} is the initial distance between the two spots. Here, the error term E has been neglected.

The instantaneous CLTE is defined as

$$\alpha_L = \frac{1}{l_{sample}} \frac{dl_{sample}}{dT}, \tag{2.4}$$

where T is the temperature in K and l_{sample} denoting the initial length of the sample in m [5]. Since dealing with homogenous materials which are unconstrained and have zero stress components, the thermal strain is the only strain to be observed. Therefore, we can simply rewrite the equation above in order to get the following relationship between the estimated strain and the CLTE

$$\alpha_L = \frac{d\varepsilon}{dT}. \tag{2.5}$$

Applying the results from equation 2.3 it follows that the CLTE is given by

$$\alpha_{\mathrm{L}} = \frac{\mathrm{d}\left(\frac{-M \cdot (A_{y,\mathrm{Upper}} - A_{y,\mathrm{Lower}})}{d_{\mathrm{ul}}}\right)}{\mathrm{d}T}. \tag{2.6}$$

3 Measurement setup

The measurement setup, depicted in Fig. 3.1, consists of four components which correspond to the ones presented in the general setup in Fig. 2.1. Two LDs with maximum power outputs of 5 mW serve as coherent light sources. Each diode illuminates a small circular region on the sample. One of these regions is located in the upper and one in the lower half of the sample. The upper LD has a center wavelength of 657 nm whereas the center wavelength of the lower one was determined to be at 655 nm. The measurement for the center wavelength has been carried out with the help of a Hamamatsu TM-CCD series mini-spectrometer which has a wavelength resolution of 1 nm.

The two illuminated spots are imaged through a telecentric optical system with demagnification $M = 1.000$. Therefore, according to equation 2.3, every shift of the illuminated surface directly translates to the same shift in the image plane although in opposing direction. The telecentric imaging system also ensures that the minimum speckle size in the image plane is large enough to not cause spatial aliasing effects. The minimum speckle size is defined by the smallest optical aperture and the laser wavelength.

The camera is a 3000 pixel line scan CCD camera with a pixel pitch, the distance between the center of two of adjacent pixel, of 7 µm. The CCD is driven directly by a Linux system running the preempt_rt patch, enabling real-time functionalities, for Ubuntu 20.04 in order to minimize variations of the exposure time which can also lead to falsely detected shifts of the patterns. Variations of $\Delta t_{\mathrm{exposure}} < 1\,\mu\mathrm{s}$ have been achieved. This limit is only exceeded in very few occasions.

The sample, depicted on the right side of Fig. 3.1, is mounted on a 2-dimensional axis so that positioning of the surface in the focus of the optics can be achieved. In order to measure the samples temperature a Pt-1000, placed in a bore in the sample, is utilized.

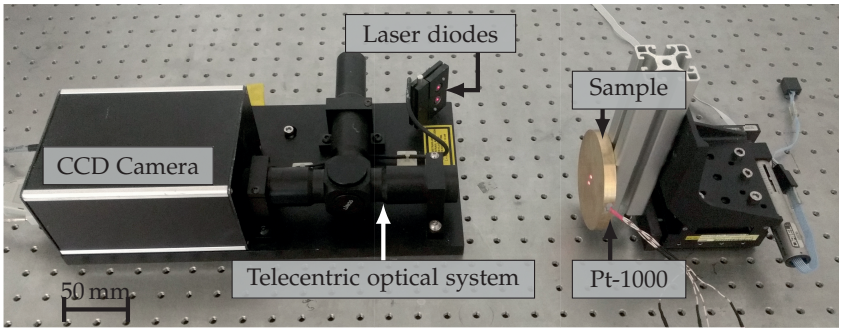

Figure 3.1: Measurement setup using telecentric imaging.

4 Signal processing and results

In this section the signal processing applied in order to estimate the CLTE will be discussed.

In Section 2 it becomes evident, that for the CLTE estimation high resolution, in the range of 100 nm, of the speckle pattern shift is crucial. Hence, the main goal of the applied signal processing techniques is to determine the pattern shift as accurately as possible. The routine described below is executed for both spots independently. Therefore, a region of interest (ROI) for each spot is chosen. The ROI for the upper spot, which is a subset of one line captured by the CCD, is depicted in Fig. 4.1.

In order to accurately estimate the pattern shift, the cross power spectral density (CPSD) $S_{xy}(f)$ as well as the coherence function $\rho(f)$ are utilized. According to the Fourier shift theorem, the argument of the complex valued CPSD encodes the space-lag of the image. The CPSD can be calculated by the following equation

$$S_{xy}(f) = E\left\{\mathcal{F}\left\{x(m)\right\}\mathcal{F}\left\{x(m+i)\right\}^*\right\}, \tag{4.1}$$

with the expected value $E\{\cdots\}$ and $\mathcal{F}\{\cdots\}$ denoting the (fast) Fourier transform (FFT) of two different lines $x(m)$ and $x(m+i)$, captured by the CCD camera at two different points in time m and $m+i$ [6]. In order to minimize the variance of the estimate of the CPSD, Welch's

method is applied. This method includes averaging over multiple periodograms of potentially overlapping sub-signals. In Fig. 4.1 this concept of splitting the signals into i sub-signals of length N_{FFT} and N_{OL} overlapping pixels is shown. However, there is a trade-off to be made. The more sub-signals i are used, the lower the variance of the resulting coefficients is. In turn, since the signal only consists of a finite amount of sample points, the number of frequencies that are calculated are reduced, too [7].

It follows, that the spatial shift A_{y} of either of the two spots based on the phase $\theta = \arg\left(S_{\mathrm{xy}}\right)$ of the CPSD is given by

$$A_{\mathrm{y}} = d_{\mathrm{pixel}} \cdot \frac{\theta N_{\mathrm{FFT}}}{2\pi f k}. \tag{4.2}$$

This can also be interpreted as a spatial group-delay, which can be assumed to be constant for the application to shifts in speckle patterns. Therefore, higher spatial frequencies also experience a larger phase-delay. For the evaluation of the space-lag based on the $k-$th spectral line, the pixel pitch d_{pixel} and the number of points used for the calculation of the FFT N_{FFT} are needed.

In order to improve the estimation, weighting of the spectral lines of the CPSD is introduced. Each spectral line of the CPSD is weighted with its corresponding squared coherence value $0 \leq |\rho(f_k)|^2 \leq 1$. The coherence function between two signals can be calculated by the relationship

$$\rho(f) = \frac{S_{\mathrm{xy}}(f)}{\sqrt{S_{\mathrm{xx}}(f) \cdot S_{\mathrm{yy}}(f)}}, \tag{4.3}$$

where $S_{\mathrm{xx}}(f)$ and $S_{\mathrm{yy}}(f)$ are the power spectral densities for line $x(m)$ and $x(m+i)$, respectively. The coherence function is a measure of the degree to which both lines in question are related by a linear time-invariant transform [6]. Especially in the case at hand, one could alternatively view a spectral line with low coherence as having less cause and effect but more noise to determine the actual phase value. Hence, additionally to weighting, a spectral line with a coherence value undercutting a predefined minimum, here $\rho_{\mathrm{min}} = 0.99$, is not being considered further for the calculation of the shift.

Further improvements can be made, if for the calculation of the shift $A_y(m, m+1)$ between line m and line $m+1$ not only these two lines but all lines $m-j, m-j+1, \cdots m, \cdots m+j-1, m+j$ are considered. In Fig. 4.1 lines $m-2, \cdots, m+3$ are depicted. Since the time between capturing each of these lines is comparably small it is assumed that the associated shift between the lines is (i) linear as a function of time and (ii) sufficiently small. The pattern shifts $A_y(m, m-j) \cdots A_y(m, m+j)$

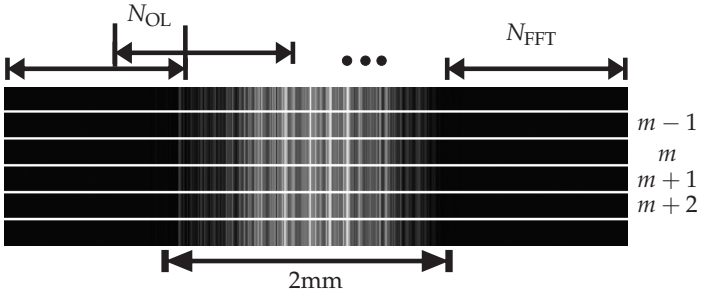

Figure 4.1: Speckle pattern in the ROI of the upper spot, taken at different points in time $m+j$.

can then be used to estimate a polynomial of first order describing the shift over time. This in turn, evaluated at t_{m+1} results in the final estimate of the shift between line m and $m+1$. This concept is visualized in Fig. 4.2. The empty circles (left) represent the pattern shifts $A_y(m, m-j) \cdots A_y(m, m+j)$ whereas the dashed line is the polynomial of first order. The resulting shift then transfers to the total shift over time depicted on the right side.

Applying the previously described signal processing routine, the results in Fig. 4.3 have been obtained. A brass sample was heated up to about 110 °C using a heat-gun. Then, as can be seen in the left graph, the sample slowly cooled down to about room temperature. As expected, the specimen shrinks at approximately the theoretical rate, depicted in grey. However, as can be seen, the estimated shift is always lower than the theoretical shift. The reason for this lies within an observable bias of the estimator, which still needs further research and potentially the introduction of a more precise model of the influence of the CCD camera. Despite the bias, the estimated averaged CLTE $\alpha_{L,25-110}$

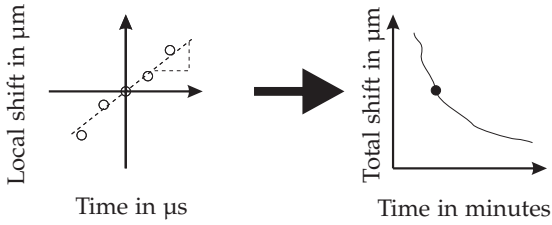

Figure 4.2: Local pattern shifts $A_y(m, m+j)$ translate to a point in the total pattern shift when evaluation of the linear polynomial at $t_{m,m+1}$ is carried out.

over the whole temperature range, based on the linearised total shift, seen on the right of Fig. 4.3, is in good agreement with the CLTE found in literature. For a smaller temperature range of 25 °C–50 °C a result closer to the theoretical one has been obtained. The values are as follows: $\alpha_{\mathrm{L,Theo}} = 18.7\,\mathrm{ppm/°C}$ [8], $\alpha_{\mathrm{L},25-110} = 17.8\,\mathrm{ppm/°C}$, $\alpha_{\mathrm{L},25-50} = 18.2\,\mathrm{ppm/°C}$.

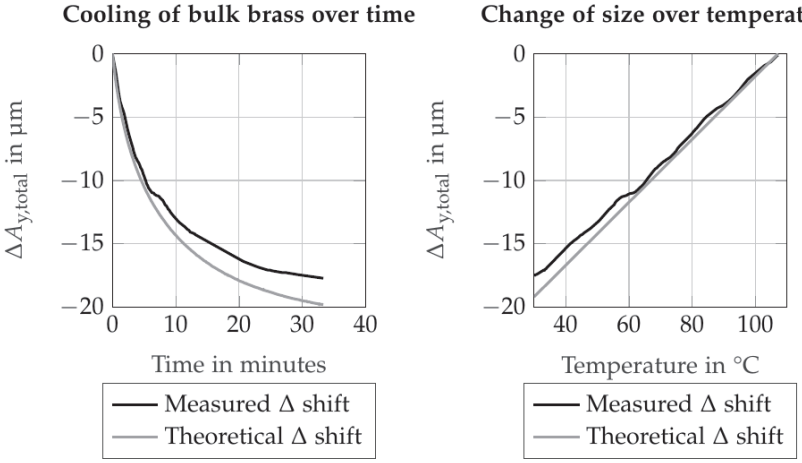

Figure 4.3: Comparison of the estimated difference $\Delta A_y = -A_{y,\mathrm{Upper}} + A_{y,\mathrm{Lower}}$ based on measurements vs. theoretical values for a bulk brass specimen. ΔA_y is essential for the calculation of the CLTE.

5 Conclusions

We have shown, that it's possible to get good estimates for the CLTE of metals evaluating the CPSD weighted by the cause-and-effect measuring coherency function. The described signal processing routine leads to acceptable results presented for the case of bulk brass and can be extended to thin specimen as well. It has been observed that with the presented estimator resulting shifts are always smaller than the ones obtained by literature based calculations. Further research is needed in order to describe this phenomenon accurately and also improve the estimate.

References

1. B. G. Zagar and C. Kargel, "A laser-based strain sensor with optical preprocessing," *IEEE Transactions on Instrumentation and Measurement*, vol. 48, no. 1, pp. 97–101, 1999.
2. R. S. Sirohi, *Speckle metrology*. New York: Dekker, 1993.
3. I. Yamaguchi, "A laser-speckle strain gauge," *Journal of Physics E: Scientific Instruments*, vol. 14, no. 11, pp. 1270–1273, 1981.
4. B. Zagar and J. Lettner, "A discussion of sources of error in laser-speckle based systems," *Proceedings of SPIE - The International Society for Optical Engineering*, vol. 8306, pp. 5–, 09 2011.
5. Tipler, *Physik*. Springer Berlin Heidelberg, 2015.
6. W. A. Gardner, *Introductionn to random processes: With applications to signals and systems*, 2nd ed. New York: McGraw-Hill, 1990.
7. P. Welch, "The use of fast fourier transform for the estimation of power spectra: A method based on time averaging over short, modified periodograms," *IEEE Transactions on Audio and Electroacoustics*, vol. 15, no. 2, pp. 70–73, 1967.
8. R. Corruccini and J. Gniewek, *Thermal Expansion of Technical Solids at Low Temperatures: A Compilation from the Literature*, ser. Monograph 29 Series. U.S. Department of Commerce, National Bureau of Standards, 1961.